Coherent vibrational dynamics during ultrafast photoinduced electron–transfer reactions: Quantum dynamical simulations within multilevel Redfield theory

ARTICLE *in* CHEMICAL PHYSICS LETTERS · JANUARY 2004

Impact Factor: 1.9 · DOI: 10.1016/j.cplett.2003.11.088

2 AUTHORS, INCLUDING:

Dassia Egorova
Christian-Albrechts-Universität zu Kiel
36 PUBLICATIONS **621** CITATIONS

Available online at www.sciencedirect.com
SCIENCE DIRECT®
Chemical Physics Letters 384 (2004) 157–164
CHEMICAL PHYSICS LETTERS
www.elsevier.com/locate/cplett

Coherent vibrational dynamics during ultrafast photoinduced electron-transfer reactions: quantum dynamical simulations within multilevel Redfield theory

Dassia Egorova *, Wolfgang Domcke

Institute of Physical and Theoretical Chemistry, Technical University of Munich, Lichtenbergstr. 4, D-85748 Garching, Germany

Received 31 July 2003; in final form 24 November 2003

Abstract

Multilevel Redfield theory is employed in order to rationalize the origin of vibrational coherences arising during ultrafast photoinduced electron-transfer (ET) reactions in polyatomic systems. After a photoexcitation to a locally-excited state, relaxation to the ground state is supposed to occur via an intermediate charge-transfer state. Stationary and nonstationary initial conditions are considered. It is shown that wave-packet motion in the ground state may be initialized not only by the laser excitation, but also by the reaction itself.

1. Introduction

Ultrafast photoinduced electron-transfer (ET) reactions in the condensed phase represent a field of intensive research within femtosecond chemistry. Observations of oscillatory structures in time-resolved spectroscopic signals, which reflect nonstationary wave-packet motion in underdamped vibrational modes, are a common feature of femtosecond ET experiments [1–6].

It is well-known that coherent vibrational motion may be created by femtosecond laser pulses in the excited electronic state as well as in the electronic ground state if there is a significant displacement between the equilibrium geometries of the optically coupled states. The excitation of coherent vibrational motion in the electronic ground state by short optical pulses is known as the stimulated resonance-Raman (RR) effect [7]. If coherent vibrational motion is detected in pump-probe signals associated with a photo-induced reaction, the question often arises whether the vibrational coherence is due to conventional Franck–Condon activity of the optical transition or whether it reflects motion along the reaction coordinate (of an isomerization reaction, for example). There are examples of ET reactions in the recent literature where it seems that the observed wave-packet motion in the electronic ground state is the result of its repopulation, i.e., of the ET reaction itself [1,3,5,6].

Furthermore, there is experimental evidence of ground-state vibrational motion arising during ET reactions at frequencies which are not present in the excited-state dynamics. For example, femtosecond pump-probe experiments on plastocyanin [5] (photoinduced ligand-to-metal charge transfer) show that a low-frequency component, which is not observed in the RR experiments on this system [8], is involved in the coherent recovery of the ground-state population. The RR inactivity of the mode suggests that there is no coordinate displacement between equilibrium geometries of the ground and initially excited electronic states along this coordinate. Hence, no moving wave-packet can be prepared in the excited state and the coherent vibrational motion in the ground state cannot be induced by the laser excitation.

If the equilibrium geometries of the ground and locally-excited (LE) electronic states coincide, vibrational

* Corresponding author. Fax: +49-89-289-13622.
E-mail address: egorova@ch.tum.de (D. Egorova).

0009-2614/$ - see front matter © 2003 Elsevier B.V. All rights reserved.
doi:10.1016/j.cplett.2003.11.088

coherence effects in the repopulation of the ground state can occur only via one or several intermediate electronic states. In the case of the ET reaction in plastocyanin, this idea is supported by the experimental results of Fraga et al. [9] and Edington et al. [10], which suggest that the initial excited state decays via one or several lower-lying ligand-field states.

Model calculations which we present here provide insight into coherent vibrational dynamics accompanying ultrafast photoinduced ET reactions, which occur via an intermediate charge-transfer (CT) state. For this purpose, we adopt multilevel Redfield theory, which has proved to be an efficient tool for modeling of ultrafast ET reactions which are driven by vibrational motion in strongly coupled reaction modes [11–15]. Redfield theory is based on the system–bath partitioning approach, in which only few degrees of freedom of a considered problem are treated explicitly (the system), while all the others are regarded as a dissipative environment (the bath). The explicitly treated system typically comprises one or several reaction modes coupled to the electronic states which are involved in the reaction. All the other vibrational degrees of freedom are assumed to be weakly coupled to the system and are modeled, e.g., as a bath of harmonic oscillators. The perturbative treatment of the system–bath interaction leads to a relatively simple equation of motion for the reduced density matrix (RDM), which is known as the Redfield equation [16] and can be numerically solved in a rather efficient way [11,12].

Previously, we have employed multilevel Redfield theory in order to investigate effects of coherent vibrational motion for the excited-state ET in the normal and inverted regions [14]. It has been shown that wave-packet motion in the reaction modes can significantly accelerate the reaction. We did not explicitly monitor the wave-packets themselves, though such attempts have been made for similar models by Lin and co-workers [17] and by May and co-workers [18,19], employing more approximative techniques.

We also have investigated the validity of the perturbative treatment of the system–bath interaction for ET models with various system, bath and system–bath coupling parameters [15]. Agreement between the multilevel Redfield-theory description and the numerically exact reference results (obtained with the self-consistent hybrid approach [20]) has been established for weak up to intermediate values of the system–bath coupling strength. Redfield theory has been found to perform particularly well at short time scales and for models of ET in the inverted region [15].

Here, we focus on ultrafast ET reactions which occur via a CT state and wave-packet dynamics in the relevant electronic states. The origin of the vibrational coherences in the repopulated ground state is of primary interest. Previous theoretical models which explicitly included the electronic ground state concerned the back ET reactions [21–23] and assumed that the transfer occurs directly from the initially excited state back to the ground state. This implies Franck–Condon activity of the reaction mode and an initial nonequilibrium configuration of the excited state (nonstationary initial condition [14,15]). In this Letter, we consider three-electronic-states models, which allow us to describe both nonstationary and stationary preparation. Radiationless decay to the ground state is assumed to occur via a bridging CT state, which is nonadiabatically coupled to the LE as well as to the ground state. Thus the LE and ground states are not coupled directly but through the CT state. This allows to model the case of a Franck–Condon inactive reaction mode (stationary initial condition) and to observe the coherences of purely reactive origin, since no wave-packet motion is generated in the initial LE electronic state. The calculations show that the reaction via a CT state results, as expected, in a delay in the repopulation of the ground electronic state.

2. Model Hamiltonian

According to the system–bath separation scheme, the complete model Hamiltonian is written as the sum of a system and a bath Hamiltonian and a system–bath interaction operator:

$$H = H_{\mathrm{S}} + H_{\mathrm{B}} + H_{\mathrm{SB}}. \tag{1}$$

Adopting the diabatic representation for the electronic states, we define the explicitly treated system as

$$H_{\mathrm{S}} = \sum_i |\phi_i\rangle(h_i + \varepsilon_i)\langle\phi_i| + \sum_{i\neq j} |\phi_i\rangle V_{ij}\langle\phi_j|, \tag{2}$$

where the three electronic states $|\phi_i\rangle$ correspond to the ground (G), LE and CT states, involved in the reaction ($i = $ G, LE, CT). The CT state is coupled to the ground and to the LE states by nonadiabatic electronic couplings $V_{\mathrm{G,CT}}$ and $V_{\mathrm{LE,CT}}$, respectively. The ground and LE states are not coupled nonadiabatically ($V_{\mathrm{G,LE}} = 0$) but via the laser excitation. ε_i are vertical electronic excitation energies and h_i denotes the vibrational Hamiltonian pertaining to the electronic state $|\phi_i\rangle$. We assume the electronic couplings V_{ij} to be constant (independent of the vibrational coordinates) and invoke the harmonic approximation for the vibrational motion. We restrict ourselves to the single system-mode case, although the numerical treatment of up to three system modes is feasible [14]. The system vibrational Hamiltonians h_i are thus written as (hereafter $\hbar = 1$)

$$h_i = \frac{\omega_{\mathrm{S}}}{2}(P^2 + Q^2) + \kappa_i Q. \tag{3}$$

Here, Q denotes the dimensionless reaction coordinate and $P = -\mathrm{i}\frac{\partial}{\partial Q}$ is the corresponding momentum operator. The vibrational frequency of the reaction mode ω_S is assumed to be the same for all the three electronic states. The parameters κ_i describe the electronic-vibrational coupling.

The system reaction mode is assumed to be linearly coupled to a bath of harmonic oscillators

$$H_B = \sum_k \frac{\omega_k}{2}(p_k^2 + q_k^2), \tag{4}$$

$$H_{SB} = Q\sum_k g_k q_k. \tag{5}$$

The bath frequencies, dimensionless coordinates and momentum operators are denoted as ω_k, q_k and p_k, respectively, the g_k describe the system–bath coupling strength. The parameters of the bath are characterized by its spectral function

$$J(\omega) = \frac{\pi}{2}\sum_k g_k^2 \delta(\omega - \omega_k). \tag{6}$$

For the model calculations, we adopt the Ohmic spectral density [24]

$$J(\omega) = \eta\omega \mathrm{e}^{-\omega/\omega_c}, \tag{7}$$

where η is a dimensionless parameter, characterizing the system–bath coupling strength, and ω_c is a bath characteristic frequency.

3. Multilevel Redfield theory

Redfield theory for dissipative systems has been developed in the context of nuclear magnetic-resonance [16] and has been widely applied to the modeling of ultrafast processes in condensed phases in the recent years [11,14,19,25–31]. The multilevel Redfield equation for the RDM has been numerically solved at different levels of accuracy, i.e. with or without additional simplifications, such as, e.g., the stationary Redfield-tensor approximation and the secular approximation. It has been shown that the secular approximation is not generally applicable for the modeling of ultrafast coherently driven ET [14], whereas the stationary Redfield-tensor approximation generally is quite accurate [15].

The Redfield equation for the RDM is obtained from the Nakajima–Zwanzig equation [32] employing the Born and Markov approximations in the dissipation description as well as the system-eigenstate representation (see, e.g. [13,15] for details of the derivation of Eq. (8)):

$$\frac{\partial\sigma_{\mu v}(t)}{\partial t} = -\mathrm{i}\omega_{\mu v}\sigma_{\mu v}(t) + \sum_{\kappa\lambda} R_{\mu v\kappa\lambda}\sigma_{\kappa\lambda}(t). \tag{8}$$

$\sigma_{\mu v} = \langle\mu|\sigma|v\rangle$ is the RDM in the basis defined via

$$H_S|\mu\rangle = E_\mu|\mu\rangle, \tag{9}$$

and $\omega_{\mu v} = E_\mu - E_v$ are the system eigenfrequencies. The first term on the r.h.s. of Eq. (8) accounts for the isolated-system dynamics, while the dissipation is described by the last term, i.e., by the Redfield tensor $R_{\mu v\kappa\lambda}$, which is usually written as

$$R_{\mu v\kappa\lambda} = \Gamma^+_{\lambda v\mu\kappa} + \Gamma^-_{\lambda v\mu\kappa} - \delta_{v\lambda}\sum_\alpha \Gamma^+_{\mu\alpha\alpha\kappa} - \delta_{\mu\kappa}\sum_\alpha \Gamma^-_{\lambda\alpha\alpha v} \tag{10}$$

with

$$\begin{aligned}\Gamma^+_{\lambda v\mu\kappa} &= \int_0^t \mathrm{d}\tau\, \mathrm{tr}_B\{\langle\lambda|H_{SB}(\tau)|v\rangle\langle\mu|H_{SB}|\kappa\rangle\}\,\mathrm{e}^{-\mathrm{i}\omega_{\mu\kappa}\tau},\\ \Gamma^-_{\lambda v\mu\kappa} &= \int_0^t \mathrm{d}\tau\, \mathrm{tr}_B\{\langle\lambda|H_{SB}|v\rangle\langle\mu|H_{SB}(\tau)|\kappa\rangle\}\,\mathrm{e}^{-\mathrm{i}\omega_{\lambda v}\tau},\end{aligned} \tag{11}$$

where we have introduced

$$H_{SB}(\tau) = \mathrm{e}^{\mathrm{i}H_B\tau}H_{SB}\,\mathrm{e}^{-\mathrm{i}H_B\tau}.$$

The components of the Redfield tensor, (11), are generally complex and time-dependent. In the following model calculations we neglect the imaginary part of the Redfield tensor and employ the stationary Redfield-tensor approximation [15], that is we extend the upper integration limit in (11) to infinity, $t \to \infty$.

The RDM is numerically propagated in time according to Redfield equation (8) by means of a fourth-order Runge–Kutta algorithm, adopted from [33].

4. Wave-packet dynamics during ultrafast ET

In this section we present the results for ultrafast ET dynamics, obtained within the model Hamiltonian of Section 2 by solving the multilevel Redfield equation (Section 3).

The time-dependent population probabilities of the relevant diabatic electronic states,

$$P_i(t) = \mathrm{tr}\{\sigma(t)|\phi_i\rangle\langle\phi_i|\}, \tag{12}$$

where $i = \mathrm{G}$, LE, CT, as well as the wave-packet motion (the time evolution of the coordinate representation of the RDM, projected on these states) are monitored. Instantaneous excitation from the ground electronic state is assumed, i.e., at $t = 0$ a wave-packet is prepared in the LE state at the equilibrium nuclear geometry of the ground electronic state. The minimum of the ground state is assumed to be located at the coordinate origin. We consider a model representing stationary as well as nonstationary preparation (Sections 4.1 and 4.2, respectively). The stationary preparation corresponds to the case of a Franck–Condon inactive reaction mode (there is no shift between equilibrium configuration of the ground and LE electronic states). In the case of the nonstationary initial condition, a moving wave-packet is prepared in the LE electronic state.

The reaction-mode frequency is chosen as $\omega_S = 0.05$ eV and so is the bath characteristic frequency, $\omega_c = \omega_S = 0.05$ eV. The system–bath coupling parameter η is varied in the considered models in order to obtain an effective damping of the vibrational motion on the time scale of interest. The temperature is set to zero.

4.1. Stationary preparation

In this section, we consider a Franck–Condon inactive reaction mode. No moving wave-packet is thus prepared in the initially excited electronic state. If coherent vibrational motion appears in the ground electronic state after the ET, it is not initiated by the laser excitation, but by the reaction itself.

The system parameters are defined in order to insure a fast and efficient transfer from the LE to the intermediate CT state and then back to the ground state. The electron-vibrational coupling of the LE state is zero, $\kappa_{LE} = 0$, (stationary preparation) and that of the CT state is $\kappa_{CT} = 2\omega_S = 0.1$ eV. The vertical excitation energies of the LE and CT states are equal, $\varepsilon_{LE} = \varepsilon_{CT} = 5\omega_S = 0.25$ eV, so that there is no barrier between the LE and CT states and the barrier between CT and G states is very low (see the potential-energy surfaces in Fig. 1). The electronic couplings are rather substantial,

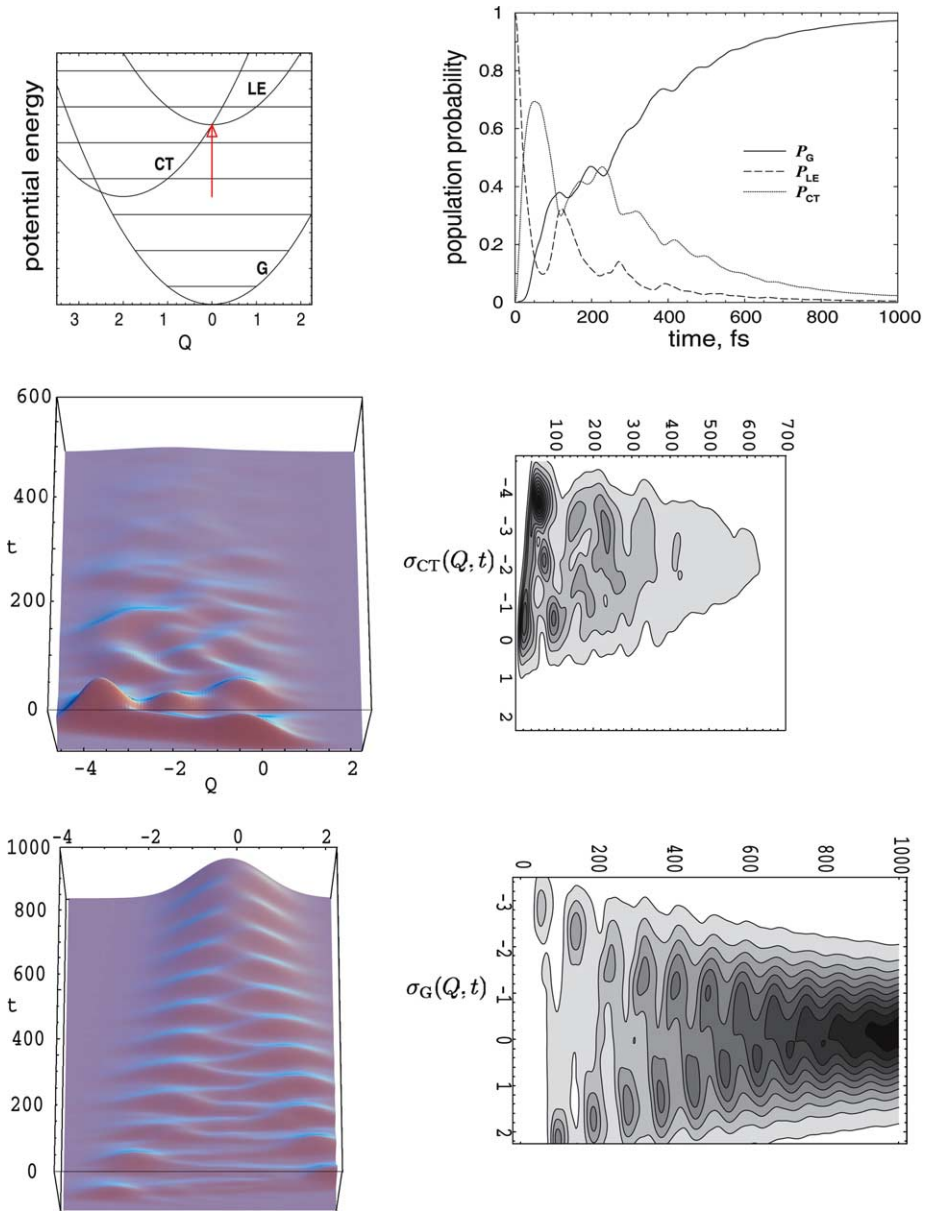

Fig. 1. Model for ultrafast ET with stationary preparation. Diabatic potential-energy surfaces, population probabilities of the locally-excited, $P_{LE}(t)$, charge-transfer, $P_{CT}(t)$, and ground, $P_G(t)$, electronic states, and wave-packet motion in the CT and G states, $\sigma_{CT}(Q,t)$, $\sigma_G(Q,t)$ in 3D and contour plots, respectively.

comparable to the system frequency ($\omega_S = 0.05$ eV): $V_{LE,CT} = 0.03$ eV, $V_{CT,G} = 0.02$ eV. The system–bath interaction is weak and determined by $\eta = 0.15$.

Fig. 1 shows the diabatic potentials for the system parameters chosen, the time-dependent population probabilities of the diabatic electronic states, $P_{LE}(t)$, $P_{CT}(t)$, $P_G(t)$, and the wave-packet motion in the CT and ground electronic states, $\sigma_{CT}(Q,t)$, $\sigma_G(Q,t)$, in three-dimensional (3D) and contour-plot representations. The LE-state projection of the RDM is not shown, as no wave-packet motion is created in this state due to the stationary initial condition. All the graphs are assembled in a manner such that the coordinate scales (potential-energy curves and wave-packets 3D plots) or the time scales (population probabilities and wave-packets contour plots) are the same.

The population probability of the LE state, $P_{LE}(t)$, exhibits electronic oscillations due to the nonadiabatic coupling $V_{LE,CT}$ which are damped on a time scale of about 400 fs. These are so-called electronic coherences, which have often been observed in various dynamical simulations of ultrafast ET, but (to our knowledge) have not yet been detected experimentally. The frequency of the beats is determined by the electronic coupling, renormalized by the Franck–Condon overlap integral of vibrational wavefunctions of the diabatic potentials.

In the CT state population, $P_{CT}(t)$, a considerable gain is observed at $t \simeq 50$ fs. One can see electronic coherences at early times, which are then modulated by higher-frequency oscillations. This modulations are of vibrational origin and reflect the creation of the wave-packet motion in the CT state. The familiar step structure, which has also been observed previously for various two electronic-state models of ultrafast ET [14,15,26,27,34], can be recognized in the decay of the CT population between 200 and 600 fs. It reflects periodic vibrational motion in the CT state: The fast decay of $P_{CT}(t)$ occurs when the wave-packet is localized in the vicinity of the crossing of the diabatic CT and G states, while the population remains constant when the wave-packet is far from the crossing point. This interpretation is confirmed by the 3D and contour-plot graphs of the $\sigma_{CT}(Q,t)$. Appearing in the vicinity of the crossing point with the LE potential (at $Q = 0$), the wave-packet in the CT state is strongly driven to the minimum of the corresponding potential ($Q = -2$), starts to move periodically and disappears rapidly because of the back transfer to the ground state.

Despite the stationary preparation, pronounced coherent vibrational motion is observed in the ground electronic state (lower part of Fig. 1). It is reflected as step structure in the increase of the ground-state population, $P_G(t)$, and is well seen in the 3D and contour plots of $\sigma_G(Q,t)$. The rather large initial amplitude of the oscillations is determined by the location of the crossing of the CT and ground-state diabatic potentials. The vibrational motion is damped due to the interaction with the bath modes and the system relaxes to the ground vibrational state within about 1 ps.

The model calculations demonstrate that coherent wave-packet motion in the ground state can be observed which is purely initiated by the reaction process. The experimental observation of coherent excitation of RR inactive modes in the ground-state vibrational dynamics is an indicator that there must be at least three electronic states involved in a ET reaction.

The essential conditions for the occurrence of coherent ground-state vibrational motion due to electron transfer are: (i) substantial electron-vibrational coupling of the underdamped reaction mode in the intermediate CT state and (ii) strong nonadiabatic coupling of this state to the LE and ground states.

4.2. Nonstationary preparation

In this section, we consider a three-electronic-state model with a nonstationary initial condition. Such a preparation is natural for two-electronic-state (donor–acceptor) back ET, but can, of course, also take place in a stepwise reaction via a bridge state.

At $t = 0$, a wave-packet is placed on the diabatic potential of the LE state at the origin of the vibrational coordinate. A nonequilibrium distribution is created due to the electron-vibrational coupling of the LE state $\kappa_{LE} = 2\omega_S = 0.1$ eV. The electron-vibrational coupling of the CT state is $\kappa_{CT} = \omega_S = 0.05$ eV and the vertical excitation energies are chosen as $\varepsilon_{LE} = 5\omega_S = 0.25$ eV, $\varepsilon_{CT} = 1.5\omega_S = 0.075$ eV. A moderate electronic coupling between the LE and CT states, as well as between the ground and CT states, has been chosen, $V_{LE,CT} = V_{CT,G} = \omega_S/5 = 0.01$ eV, which appears to be sufficient for the effective transfer.

The nonstationary preparation results in an excess in vibrational energy and coherent vibrational motion in the initially prepared (LE) electronic state. To damp this initial vibrational coherence on a time scale of a few hundred fs, a stronger system–bath coupling than in the previously considered model (Section 4.1) is required. The system–bath interaction strength is thus set to $\eta = 0.5$. Redfield theory has been shown to be physically meaningful in this regime [15].

The diabatic potentials, the population probabilities of the three diabatic states, $P_{LE}(t)$, $P_{CT}(t)$, $P_G(t)$, as well as the projections of the coordinate representation of the RDM to these states, $\sigma_{LE}(Q,t)$, $\sigma_{CT}(Q,t)$, $\sigma_G(Q,t)$, are shown in Fig. 2. The coordinate/time scales of the graphs are the same.

The initial system evolution is characterized by a step-like decay of $P_{LE}(t)$ (dashed curve in the population-probability graph), as observed previously in two-electronic-state models [14,15,26,27,34]. The step structure reflects coherent wave-packet motion in the LE

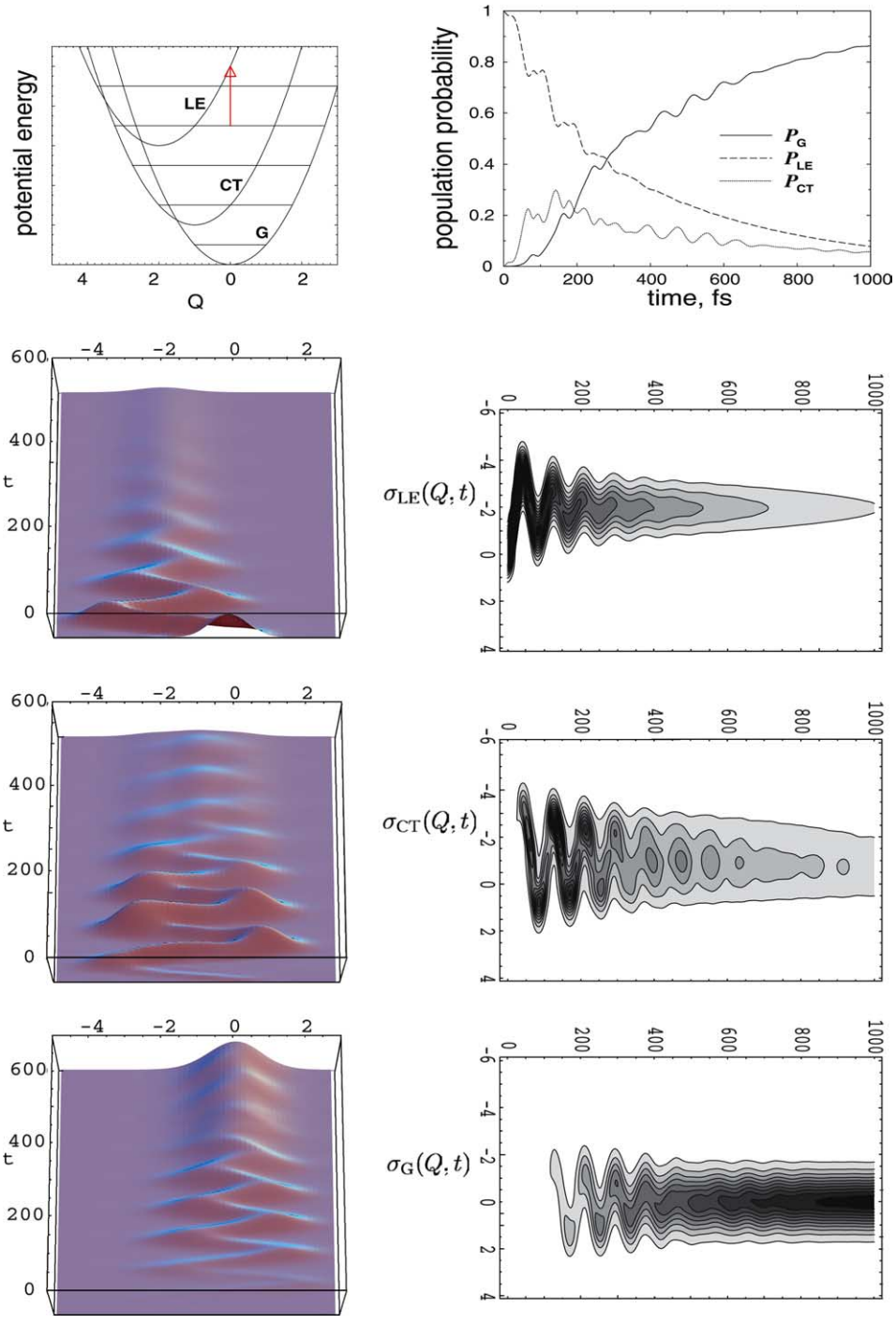

Fig. 2. Model for ultrafast ET with nonstationary preparation. Diabatic potential-energy surfaces, population probabilities of the locally-excited, $P_{LE}(t)$, charge-transfer, $P_{CT}(t)$, and ground, $P_G(t)$, electronic states, and wave-packet motion in these states, $\sigma_{LE}(Q,t)$, $\sigma_{CT}(Q,t)$, $\sigma_G(Q,t)$ in 3D and contour plots, respectively.

electronic state: a fraction of the wave-packet is transferred to the CT state each time the moving wave-packet hits the crossing region. This interpretation is confirmed by the 3D and contour-plot graphs of $\sigma_{LE}(Q,t)$. The wave-packet in the LE state exhibits damped vibrational motion with a loss of the population to the CT state. This motion is quenched after ~400 fs due to vibrational relaxation. Due to the low barrier, the crossing point is still accessible, even when the wave-packet has relaxed to the minimum of the LE-state potential ($Q = -2$), and a further monotonous decay of the LE-state population is observed. In contrast to the model of Section 4.1, no electronic coherences are observed in the LE-state dynamics. The reason for it is a weaker electronic coupling

and a stronger damping, compared to the model of Section 4.1.

The population dynamics of the CT state reflects a competition between the gain of population from LE state and its loss to the ground electronic state. The population probability of this state, $P_{CT}(t)$ (dotted curve in the population-probability graph), increases up to ~300 fs, but after this time the loss to the ground state is not longer compensated by the gain from the LE state. The wave-packet in the CT state, $\sigma_{CT}(Q,t)$, appears in the vicinity of the crossing point with the LE state and its periodical motion survives on approximately the same time scale as that in the LE state (see contour plots of $\sigma_{CT}(Q,t)$ and $\sigma_{LE}(Q,t)$). After relaxation to the minimum of the diabatic potential of the CT state, amplitude modulations of the wave-packet can be recognized in the 3D and contour-plot graphs of $\sigma_{CT}(Q,t)$. In the population dynamics they express themselves as the oscillatory structure of $P_{CT}(t)$ between ~400 and ~800 fs.

Coherent wave-packet motion in the ground state becomes visible at $t \simeq 100$ fs. The initial amplitude of the oscillations is determined by the location of the crossing of the ground state with the CT state and is slightly smaller than that in the LE and CT states. The oscillations are efficiently damped at ~400 fs time scale, but small-amplitude vibrational motion survives up to ~800 fs (see the contour plot of $\sigma_G(Q,t)$ in Fig. 2). The population probability of the ground state, $P_G(t)$ (solid line in the population-probability graph), increases until ~400 fs. It exhibits oscillations which are a mirror image of the oscillations of $P_{CT}(t)$ between ~400 and ~800 fs. Since vibrational motion is efficiently damped after ~400 fs, these modulations probably are of the electronic origin and their frequency is determined by the adiabatic energy gap between CT and ground-state potentials [35], which is 0.05 eV in this model example.

The calculations demonstrate that the ET dynamics for this model is characterized by the consecutive transfer of the laser-induced coherent wave-packet motion from the LE to the CT and then to the ground state. Transfer of vibrational coherences between diabatic states has been observed previously for the two-electronic-state models of ultrafast ET [26]. The present three electronic-state calculations show that coherent vibrational motion can survive several sequential nonadiabatic processes. It is thus conceivable that coherent vibrational dynamics can play an essential role in long-range ET via several bridge states, for example in photosynthetic reaction centers or in electronic transport through molecular wires.

5. Conclusions

We have employed multilevel Redfield theory to model ultrafast photoinduced ET reactions which occur in a stepwise manner via an intermediate CT state. Models with stationary and nonstationary preparation (i.e., with nonequilibrium and equilibrium nuclear geometry in the initial (LE) electronic state at $t = 0$) have been investigated. Wave-packet motion in the ground state has been observed in the both cases, though the origin of the vibrational coherence is different.

An excess in vibrational energy and coherent vibrational motion is generated by nonstationary preparation. The coherent vibrational motion is gradually transfered from the initial LE state to the intermediate CT and then (after approximately 100 fs) to the ground electronic state.

On the other hand, no wave-packet motion is generated in the LE state in the case of a Franck–Condon inactive reaction mode (stationary initial condition). However, a moving wave-packet can be created in the the ground electronic state after its repopulation via the CT state.

While in the model with nonstationary initial condition the main effect of the CT bridge state is a certain delay in the repopulation of the ground state, the presence of at least one intermediate electronic state with strongly shifted equilibrium geometry is crucial in the stationary-preparation model. In this case the vibrational coherence in the electronic ground state is generated by the ET reaction itself.

References

[1] K. Wynne, G.D. Reid, R.M. Hochstrasser, J. Chem. Phys. 105 (1996) 2287.
[2] I. Rubtsov, K. Yoshihara, J. Phys. Chem. A 103 (1999) 10202.
[3] S. Engleitner, M. Seel, W. Zinth, J. Phys. Chem. 103 (1999) 3013.
[4] P. Kambhampati, D.H. Son, T.W. Kee, P.F. Barbara, J. Phys. Chem. A 104 (2000) 10637.
[5] S. Nakashima, Y. Nagasawa, S.K.T. Okada, M. Sato, T. Kohzuma, Chem. Phys. Lett. 331 (2000) 396.
[6] D.H. Son, P. Kambhampati, T.W. Kee, P.F. Barbara, J. Phys. Chem. A 106 (2002) 4591.
[7] S. Mukamel, Principles of Nonlinear Optical Spectroscopy, University Press, Oxford, 1995.
[8] M.A. Webb, C.M. Kwong, G.R. Loppnow, J. Phys. Chem. B 101 (1997) 5062.
[9] E. Fraga, M.A. Webb, G.R. Loppnow, J. Phys. Chem. 100 (1996) 3278.
[10] M.D. Edington, W.M. Diffey, W.J. Doria, R.E. Riter, W.F. Beck, Chem. Phys. Lett. 275 (1997) 119.
[11] J.M. Jean, R.A. Friesner, G.R. Fleming, J. Chem. Phys. 96 (1992) 5827.
[12] W.T. Pollard, R.A. Friesner, J. Chem. Phys. 100 (1994) 5054.
[13] W.T. Pollard, A.Y. Felts, R.A. Friesner, Adv. Chem. Phys. XCIII (1996) 77.
[14] D. Egorova, A. Kühl, W. Domcke, Chem. Phys. 268 (2001) 105.
[15] D. Egorova, M. Thoss, H. Wang, W. Domcke, J. Chem. Phys. 119 (2003) 2761.
[16] A.G. Redfield, Adv. Magn. Reson. 1 (1965) 1.
[17] M. Sugawara, M. Hayashi, S. Suzuki, S.H. Lin, Mol. Phys. 57 (1996) 637.
[18] V. May, O. Kühn, M. Schreiber, J. Phys. Chem. 97 (1993) 12591.

[19] O. Kühn, V. May, M. Schreiber, J. Chem. Phys. 101 (1994) 10404.
[20] H. Wang, M. Thoss, W.H. Miller, J. Chem. Phys. 115 (2001) 2979.
[21] B. Wolfseder, W. Domcke, Chem. Phys. Lett. 259 (1996) 113.
[22] C. Fuchs, M. Schreiber, J. Chem. Phys. 105 (1996) 1023.
[23] H. Wang, M. Thoss, J. Phys. Chem. A 107 (2003) 2126.
[24] A.J. Leggett, S. Chakravarty, A.T. Dorsey, M.P.A. Fisher, A. Garg, W. Zwerger, Rev. Mod. Phys. 59 (1987) 1.
[25] A.K. Felts, W.T. Pollard, R.A. Friesner, J. Phys. Chem. 99 (1995) 2929.
[26] J.M. Jean, J. Chem. Phys. 104 (1996) 5638.
[27] J.M. Jean, J. Phys. Chem. A 102 (1998) 7549.
[28] A. Matro, J.A. Cina, J. Phys. Chem. 99 (1995) 2568.
[29] D. Segal, A. Nitzan, W.B. Davis, M.R. Wasielewsky, M.A. Ratner, J. Phys. Chem. B 104 (2000) 3817.
[30] A. Kühl, W. Domcke, J. Chem. Phys. 116 (2002) 263.
[31] S. Hahn, G. Stock, J. Chem. Phys. 116 (2002) 1085.
[32] R. Zwanzig, J. Chem. Phys. 33 (1960) 1338.
[33] W.A. Press, S.A. Teukolsky, W.T. Vetterling, B.P. Flannery, Numerical Recipes in Fortran – The Art of Scientific Computing, second edn., Cambridge University Press, Cambridge, 1992.
[34] B. Wolfseder, L. Seidner, G. Stock, W. Domcke, Chem. Phys. 217 (1997) 275.
[35] M. Thoss, W. Domcke, Chem. Phys. 296 (2004) 217.